

Quantitative Magnetization Transfer Imaging With Non-Exchanging Compartment Modeling: From CSF Partial Volume Correction to More Accurate Characterization of White Matter?

Pouria Mossahebi¹, Andrew L Alexander^{2,3}, Aaron S Field^{1,4}, and Alexey A Samsonov⁴

¹Biomedical Engineering, University of Wisconsin, Madison, WI, United States, ²Medical Physics, University of Wisconsin, Madison, WI, United States, ³Waisman Lab for Brain Imaging and Behavior, University of Wisconsin, Madison, WI, United States, ⁴Radiology, University of Wisconsin, Madison, WI, United States

INTRODUCTION: Quantitative magnetization transfer imaging (qMTI) [1] provides unique parameters sensitive to macromolecular tissue composition, which is useful for assessing pathological tissue conditions [2-3]. The majority of *in vivo* qMTI methods are based on a two-pool model, in which macromolecular protons (bound pool) are assumed in exchange with free water protons (free pool). The two-pool MT model often provides a reasonable tradeoff between accuracy of complex MT models [4] and feasibility of *in vivo* application [5]. However, at typical MRI resolutions, the two-pool model is inadequate to describe the signal behavior with partial volume effects (PVE) with non-exchanging compartments such as cerebrospinal fluid (CSF) [6,7]. The presence of non-exchanging or very slowly exchanging compartments will underestimate key qMT parameters, especially in gray matter (GM) where significant CSF PVE exists [6,7]. To minimize PVE effects in qMT measurements, we propose an extended MT model where a two-pool MT subsystem is augmented by a third, non-exchanging (NE) pool.

THEORY: The additional NE pool was modeled using the formalism of a previously proposed modified cross-relaxation imaging (mCRI) approach [1,8]. This approach acquires SPGR data with varying excitation flip angles (α) (VFA) and MT-weighted SPGR data with several combinations of off-resonance frequencies (Δ) and powers (α_{MT}) of MT saturation pulse, which are fit simultaneously to the unified signal model $s = S_{\alpha, \Delta, \alpha_{MT}}^{MT}(M_0, R1_F, f, k, T_2^B)$ to yield bound pool fraction f , longitudinal relaxation rate $R1_F$, cross-relaxation rate k , transverse relaxation time of the bound pool T_2^B , and proton density term M_0 (Fig. 1). In the absence of direct saturation due to off-resonance irradiation ($\Delta > 2.5$ kHz) [9], the signal from NE pool is independent of Δ and α_{MT} and may be described by a standard single pool SPGR signal equation. Therefore, the compartment contributes to the total signal in additive fashion: $s = S_{\alpha, \Delta, \alpha_{MT}}^{MT}(M_E, R1_F, f, k, T_2^B) + S_{\alpha}^{SPGR}(M_{NE}, R1_{NE})$ [Eq. 1],

where $M_E = M_F + M_B$, $R1_F$, M_{NE} , and $R1_{NE}$ are proton density and longitudinal relaxation rate of exchanging subsystem and non-exchanging pool. The resulting NE-mCRI method fits an extended set of VFA and MT measurements to the signal equation to yield all seven parameters describing both exchanging subsystem and non-exchanging pool (Fig. 1).

METHODS: The appropriate experimental design was first determined using Monte-Carlo simulations. The standard mCRI protocol (VFA: FAs $\alpha = [5, 10, 20, 30]^\circ$, MT SPGR: $\alpha = 10^\circ$, $\Delta = 2.5, 5, 9, 13$ kHz, $\alpha_{MT} = [500, 1100]^\circ$, 18ms Fermi pulse) was extended by three MT SPGR measurements ($\Delta = 2.5$ kHz, $\alpha_{MT} = 785^\circ$) with varying $\alpha = [5, 20, 30]^\circ$. All data were acquired using a 3D MT-SPGR pulse sequence with TR/TE = 40/2.0ms, 240x180x80mm FOV, 128x96x40 matrix on a 3.0T GE MR750 scanner. Flip angle (B1) and field (B0) maps were measured by AFI [11] and IDEAL [12] to correct flip angles and offset frequencies in the subsequent processing. The mCRI processing workflow was implemented according to [8]. Parametric maps were generated by fitting all data simultaneously to Eq. [1].

RESULTS: Fig 2 shows that NE-mCRI efficiently decomposes the standard two-pool (M_0) model into exchanging and non-exchanging terms (M_E and M_{NE}), the latter showing high contrast and expected anatomical distribution for CSF. The removal of the CSF component markedly increases the apparent size of GM structures on f map in the areas with PVE from CSF (red arrow, bordering the ventricles). CSF PVE removal also significantly affects several key qMT parameters in GM (Fig. 3), especially the cross-relaxation rate k . Additional analysis was run in compact WM/GM structures that are not expected to have PVE from CSF (Table 1). Our modeling detected a non-negligible NE component in compact WM (white arrow in Fig. 2), but not in compact GM (yellow arrow in Fig. 2). The removal of this component (corrects the underestimation of f and k) increases the bound pool fraction f estimation. Similarly to CSF PVE, the cross-relaxation rate k in compact WM structures is affected most and the effect size varies according to the detected f_{NE} (Table 1). $R1$ of this NE component ($R1_{NE}$) approaches that of free water.

DISCUSSION: We demonstrated that the two-pool MT model is influenced by non- or slowly-exchanging PVE compartments, i.e. CSF. As CSF PVE may be significant for GM [6, 7], CSF may be a serious confounder for accurate characterization of GM. To compensate, we proposed a new MT model with an additional non-exchanging compartment (NE-mCRI), which removed CSF (non-exchanging) contamination from brain qMT maps. ROI analysis confirmed that CSF is a primary source of observed bias in GM qMT measures. The NE-mCRI enables direct estimation of PVE with CSF and may be potentially useful for brain atrophy measurements in multiple sclerosis and Alzheimer disease, and in older patients who often have enlarged perivascular spaces and/or chronic lacunar infarcts filled with CSF. Our NE-mCRI analysis also revealed significant regionally varying f_{NE} in compact WM (6-12%) with longitudinal relaxation rate in the range 0.25-0.36 s⁻¹. While association of the NE compartment with microscopic structures is yet to be revealed, several interesting observations can be made. WM has many free water compartments associated with axonal, myelin, and extra-axonal water, all described by a single pool in the standard two-pool model. Myelin water is expected to have the highest rate of MT exchange with macromolecular-rich myelin, mediating MT with other compartments primarily through diffusion at much lower rates. Hence, the NE pool may be considered as an approximation to such more slowly exchanging compartments. For example, the posterior limb of internal capsule (ROI with the largest detected f_{NE}) has very large axons with thick myelin sheaths compared to the majority of other brain WM structures [14]. The splenium of corpus callosum (CC) has also thicker axons compared to that of the genu of CC [15], which may explain the observed differences in corresponding f_{NE} (Table 1). Finally, the removal of such slowly exchanging components using NE approximation increased overall cross-relaxation rate k and f in those structures as expected. Given demonstrated feasibility of *in vivo* imaging, NE-mCRI may improve existing tradeoffs with 4-pool models and provide more accurate characterization of WM. Additionally; it has potential to improve accuracy of qMT in edematous conditions or in fat (non-exchanging) liver.

REFERENCES: [1] Yarnykh VL, et al. Neuroimage 2004; 23:409. [2] Underhill HR, et al. NeuroImage 2011; 54:2052. [3] Samsonov A et al. Neuroimage 2012; 62:1390. [4] Li JG, et al. MRM 1997; 37:866. [5] Stanisz GJ, et al. MRM 1999; 42:1128. [6] Deoni SC, et al. MRM 2012; in press. [7] Yang AW, et al. MRM 2012; in press. [8] Mossahebi P, et al. ISMRM 2012, 0741. [9] Portnoy S, et al. MRM 2007; 58:144. [10] Chen J, et al. MRM 2010; 63:713. [11] Yarnykh VL. MRM 2007; 57:192. [12] Reeder SB, et al. MRM 2005; 54:636. [13] Underhill HR, et al. Neuroimage 2009; 47:1568. [14] Yagishita A, et al. Radiology 1994; 191:455. [15] Aboitiz F, et al. Brain Research 1992; 598:143.

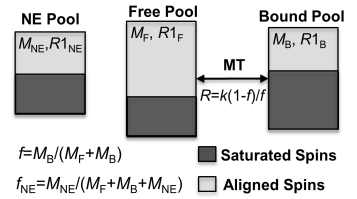


Figure 1. The proposed three-pool model.

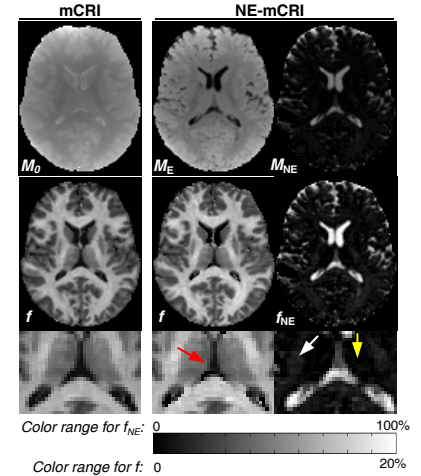


Figure 2. mCRI and NE-mCRI processing results..

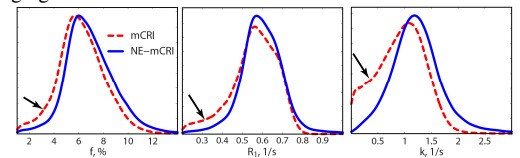


Figure 3. GM histograms of key qMT measures. Arrows point to the histogram areas most affected by CSF PVE.

Region	f_b (%)		k (s ⁻¹)		T_2^B (μ s)		$R1_{NE}$ (s ⁻¹)	f_{NE} (%)
	mCRI	NE-mCRI	mCRI	NE-mCRI	mCRI	NE-mCRI	NE-mCRI	NE-mCRI
CC, genu	14.58±0.57	15.85±0.66	2.41±0.19	3.09±0.50	10.21±0.34	10.86±0.31	0.25±0.08	6.20±2.73
CC, splenium	13.74±0.44	15.23±0.74	2.57±0.20	3.37±0.28	10.42±0.18	10.91±0.20	0.36±0.04	7.78±2.69
IC, posterior limb	13.49±0.79	15.51±1.03	1.95±0.10	2.98±0.40	12.48±0.41	12.99±0.36	0.35±0.06	12.03±2.50
Caudate nucleus	6.70±0.48	6.74±0.49	1.14±0.09	1.21±0.13	10.05±0.46	10.33±0.37	0.19±0.19	1.56±3.35
Putamen	7.78±0.40	7.99±0.43	1.37±0.07	1.39±0.10	10.44±0.30	10.82±0.31	0.16±0.07	1.01±1.10
Thalamus	8.42±0.56	8.75±0.61	1.59±0.10	1.64±0.16	10.68±0.40	11.06±0.38	0.27±0.15	2.10±2.23

Table 1. In vivo ROI measurements of qMTI parameters (CC=Corpus callosum, IC=Internal Capsule). Asterisk indicates that measurements were not statistically significant (p>0.05).

ACKNOWLEDGEMENTS:
This work was supported by NIH (R01NS065034).